Chapter 9

Real-time integration of intracardiac echocardiography and multi-slice computed tomography to guide radiofrequency catheter ablation for atrial fibrillation

Dennis W. den Uijl, Laurens F. Tops, José M. Tolosana, Joanne D. Schuijf, Serge A. Trines, Katja Zeppenfeld, Jeroen J. Bax, Martin J. Schalij.

Heart Rhythm. 2008 Oct;5(10):1403-10

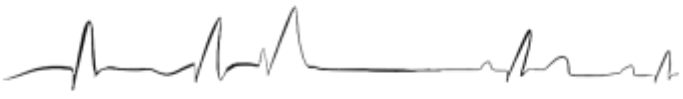

Abstract

Background: Multi-slice computed tomography (MSCT) integration is commonly used to guide radiofrequency catheter ablation (RFCA) for atrial fibrillation (AF). MSCT provides detailed anatomical information but lacks the ability to provide real-time anatomy during RFCA. Intracardiac echocardiography (ICE) allows real-time visualization of cardiac structures.

Objective: The purpose of this study was to investigate the feasibility of three-dimensional (3D) anatomical mapping of the left atrium (LA) with ICE and integrating the 3D map with MSCT to facilitate RFCA for AF.

Methods: In seventeen patients undergoing RFCA for AF, 3D mapping of the LA was performed with ICE using a new mapping system (CARTOSOUND™, Biosense Webster) which allows tracking of a new ICE probe. On each ICE image endocardial contours were traced and used to generate a 3D map of the LA and pulmonary veins (PVs). A preprocedural acquired MSCT image of the LA was then integrated with the 3D map. Additionally, PV assessment with ICE was compared with MSCT.

Results: Accurate 3D mapping could be performed in all patients with a mean number of 31.1 ± 8.5 contours. Integration with MSCT resulted in a mean distance between MSCT and ICE contours of 2.2 ± 0.3 mm for the LA and PVs together and of 1.7 ± 0.2 mm around the PV ostia specifically. Agreement in assessment of PV anatomy and diameters between ICE and MSCT was excellent.

Conclusion: 3D ICE mapping of the LA is feasible. The 3D map created with ICE can be merged with MSCT to facilitate RFCA for AF.

Introduction

Ectopic beats originating from the pulmonary veins (PVs) can initiate atrial fibrillation (AF) [1]. Radiofrequency catheter ablation (RFCA) is considered a reasonable option in the treatment of patients with AF, when at least one anti-arrhythmic drug has failed [2]. Ablation strategies targeting the PVs are the cornerstone of these RFCA procedures [2]. To plan and guide these ablation procedures, non-invasive three-dimensional (3D) imaging modalities like magnetic resonance imaging and multi-slice computed tomography (MSCT) are available to visualize the left atrium (LA) and PVs [3,4]. Electrophysiological navigation systems allowing the integration of MSCT with electroanatomical maps, combine accurate real-time navigation with detailed anatomical information thereby facilitating the ablation procedure [5] and reducing fluoroscopy time and procedural duration [6].

However, a limiting factor of using MSCT to guide the ablation procedure is the time interval between image acquisition and the ablation procedure which may result in differences in heart rhythm, heart rate and fluid status potentially causing an inaccurate registration process. Because the quality of the registration process determines the accuracy of navigating [7], this could result in less accurate lesion placement during RFCA. Recently, a new electroanatomical mapping system has been released that allows integration of 3D mapping and real-time intracardiac echocardiography (ICE). Using this system, a registered 3D shell of the LA and PV anatomy can be generated from two-dimensional (2D) ICE images.

The aim of this study was to investigate the feasibility of creating a 3D map of the LA and PVs with ICE and integrating this map with a MSCT surface image in order to facilitate RFCA for AF. In addition, a direct comparison between this new ICE technique and MSCT for the assessment of PV anatomy was performed.

Methods

Study population and protocol

The study population comprised 17 consecutive patients with symptomatic drug refractory AF, who underwent RFCA in our institution. In all patients a MSCT was acquired two days before the ablation. Prior to the procedure, the raw MSCT data was loaded into an electroanatomical mapping system (CARTO XP™, Biosense Webster, Diamond Bar, California) equipped with a newly developed image integration module (CARTOSOUND™, Biosense Webster). During the ablation procedure 3D maps of the LA and PVs were created using an ICE catheter with an imbedded CARTO navigation sensor (10Fr Soundstar™, Biosense Webster) allowing the mapping system to detect its position and generate a registered 3D shell from the recorded two-dimensional (2D) images. After completion of the mapping procedure a registration process was performed to integrate the MSCT image with the 3D map made with ICE. Thereafter the merged MSCT image and 3D maps were used to guide the RFCA procedure.

Multi-Slice Computed Tomography

In all patients MSCT data were acquired two days before the ablation procedure. The MSCT examination was performed with a 64-slice Toshiba Aquilion 64 system (Toshiba Medical Systems, Otawara, Japan) (7 patients) or a 320-slice Toshiba Aquilion One system (Toshiba Medical Systems) (10 patients). Craniocaudal scanning was performed during breath holding. For the Aquilion 64 system collimation was 64 x 0.5 mm, rotation time 400 ms and tube voltage between 100 and 135 kV at 250 to 400 mA. For the Aquilion One system collimation was 320 x 0.5 mm, rotation time 350 ms and tube voltage 120 kV at 400 to 500 mA. In all patients nonionic contrast material (Iomeron 400, Bracco, Milan, Italy; 105 ml for Aquilion 64 and 50 ml for Aquilion One scanning) was

infused through the antecubital vein at a rate of 5 ml/s followed by 50 ml saline solution flush. Automatic detection of the contrast bolus was used to time the start of the scan. Before the ablation procedure, all MSCT data were analyzed on a dedicated workstation (Vitrea 2; Vital Images, Minnetonka, Minnesota).

Image processing and segmentation

Prior to the ablation procedure, the raw MSCT data were loaded into the image integration module of the mapping system (CartoMerge™, Biosense Webster) and a segmentation process was performed. The segmentation process consisted of three phases as described previously [5]. The first step was to delineate the borders of interest on the MSCT (LA and PVs) by manually setting the threshold intensity range. A 3D volume was subsequently created of all structures within the set threshold range. The second step was to segment this 3D volume into different structures by placing markers in the middle of the different areas. An algorithm was used to automatically depict the different structures based on the placement of the markers and the border of the 3D volume. Finally, the segmented surface images were exported to the mapping system.

Anatomical mapping with intracardiac echocardiography

During the catheter ablation procedure, a 3D anatomical map was created with ICE images. A new mapping system was used, equipped with a new image integration module that allows the integration of ICE and 3D mapping (CARTOSOUND™). This system is able to detect the position and direction of a specifically designed ICE catheter with an imbedded CARTO navigation sensor located at its tip (Soundstar™). By positioning the ICE catheter inside the right atrium, ECG gated images of the LA and PVs were acquired. To provide ECG gating, either a quadripolar electrophysiological catheter placed inside the

right atrium or the body surface ECG was used as a reference signal in patients with sinus rhythm or AF, respectively. In order to correct for respiratory phase, all ICE images were acquired during expiratory breath hold.

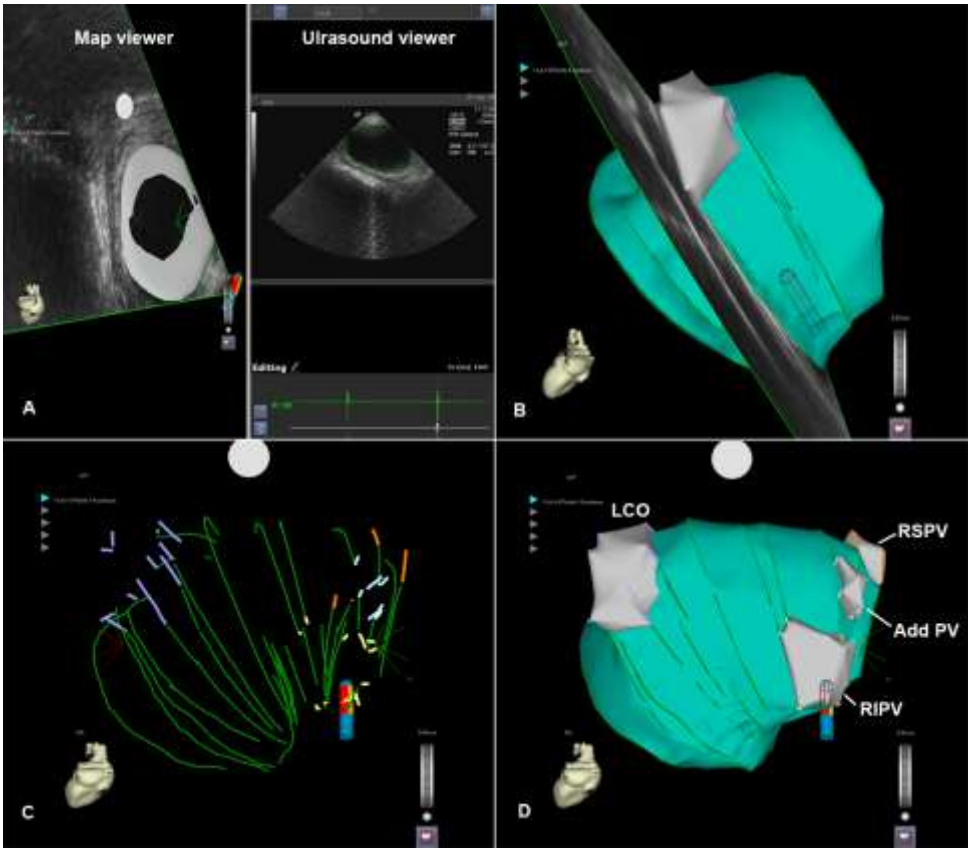

Figure 1. Three-dimensional (3D) mapping with intracardiac echocardiographic (ICE). Ultrasound images of the left atrium (LA) are acquired. The endocardial contour of the LA is traced on the ultrasound viewer of the mapping system. After assigning the contour to a map, it appears on the map viewer (A). By acquiring more contours and reconstructing them into a registered 3D shell (B), the shape of the LA and pulmonary veins (PVs) is depicted. Systematically, the LA and PVs are visualized (C) until a complete 3D map of the LA and PVs is acquired (D). Add PV = additional pulmonary vein, LCO = left common ostium, RIPV = right inferior pulmonary vein, RSPV = right superior pulmonary vein.

Intracardiac echocardiography was performed using a Sequoia ultrasound system (Siemens Medical Solutions USA, Mountain View, California)

which transferred real-time ICE data to the mapping system. On the mapping system, the endocardial contours were traced manually after which they were assigned to a map (Figure 1A). All contours within a map were used to generate a registered 3D shell (Figure 1B and 1C). For each map a separate shell was generated. Different maps were created for the LA and for each of the PVs (Figure 1D).

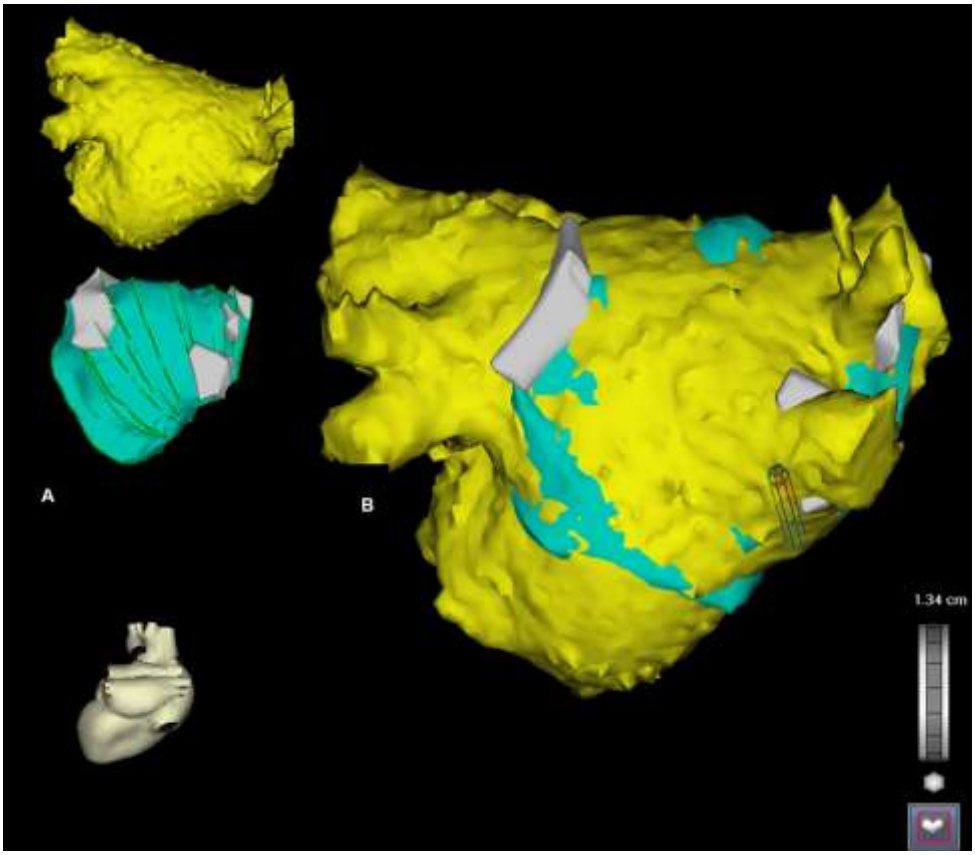

Figure 2. After three-dimensional (3D) mapping with intracardiac echocardiography, the 3D map and multi-slice computed tomography (MSCT) image are displayed next to each other (A). Then a manual registration process was performed. This resulted in the integration of the 3D map and the MSCT image in order to anatomically guide the ablation procedure (B).

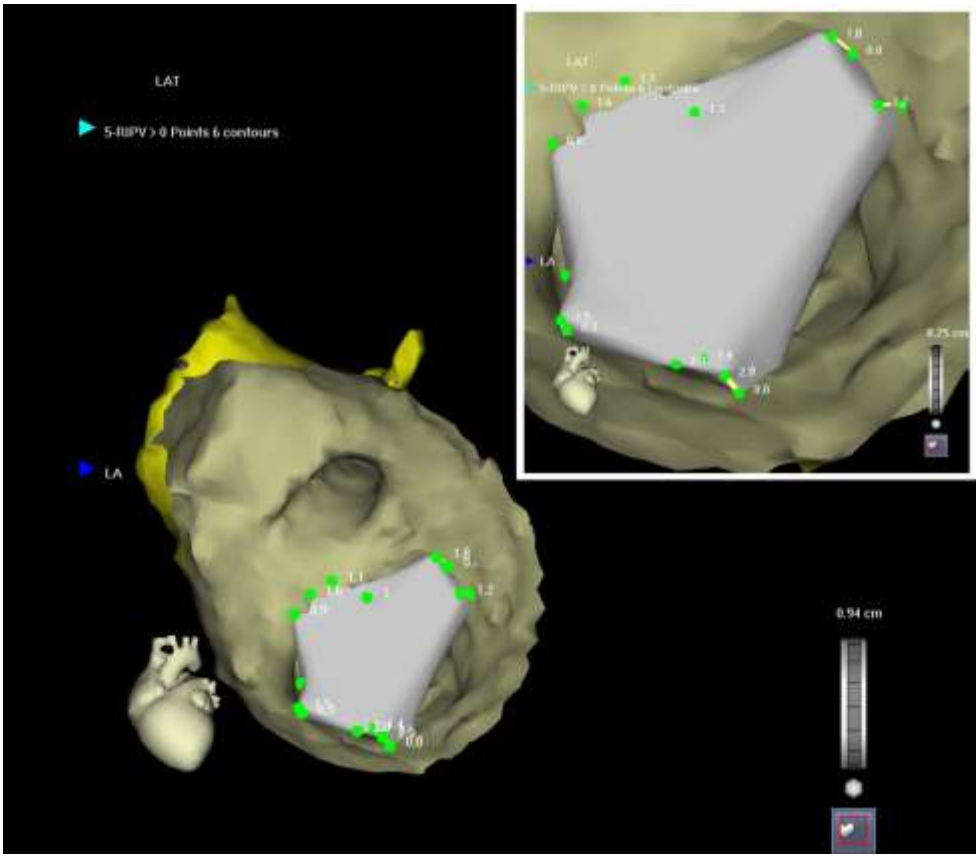

Figure 3. The quality of the registration process was reviewed at the level of the pulmonary vein ostium by measuring the distance between multi-slice computed tomography and three-dimensional map at 5 representative points.

Registration

After creating a map with ICE, a registration process was performed to integrate the MSCT surface image and the 3D map. First, the MSCT surface image was displayed next to the anatomical map (Figure 2A). A landmark was placed at a distinct anatomical structure on the anatomical map and at a corresponding point on the MSCT model. Then 'visual alignment' was performed by minimizing the distance between both landmarks. Next, the maps created during the mapping procedure were each assigned to the

corresponding MSCT surface image and a 'surface registration' was performed. During this process the ICE contours were represented as a line of adjacent mapping points. An internal algorithm was used to minimize the distance between these points and the MSCT surface image (Figure 2B).

The accuracy of the registration process was then reviewed. The mean value, standard deviation and range of the distance between the points along the ICE contours and the MSCT surface were provided by the algorithm. The accuracy of the registration process at the level of the PVs was evaluated by measuring the distance between the contours and MSCT surface at 5 representative points around each PV ostium (Figure 3).

Pulmonary vein anatomy and quantitative measurements

After an accurate registration had been acquired the PVs and their atrial insertion were evaluated on both MSCT and ICE. Pulmonary vein anatomy was classified according to the presence or absence of a common ostium/trunk and/or additional veins. As described previously, a common ostium was defined as a PV carina located outside the extrapolated endocardial border of the LA [4]. A common trunk was defined as a clearly recognizable common part in which both superior and inferior PV drain before emptying into the LA [8]. An additional vein was defined as a supranumerical vein entering the LA with a separate ostium. The same criteria for PV classification were used for MSCT and ICE evaluation.

Pulmonary vein diameters on MSCT were measured in anterior-posterior (AP) and superior-inferior (SI) direction inside the PV ostium, as previously described [4]. Pulmonary vein diameters on ICE were measured at the widest point. Left atrial diameter was measured in AP direction on both MSCT and the 3D map created with ICE.

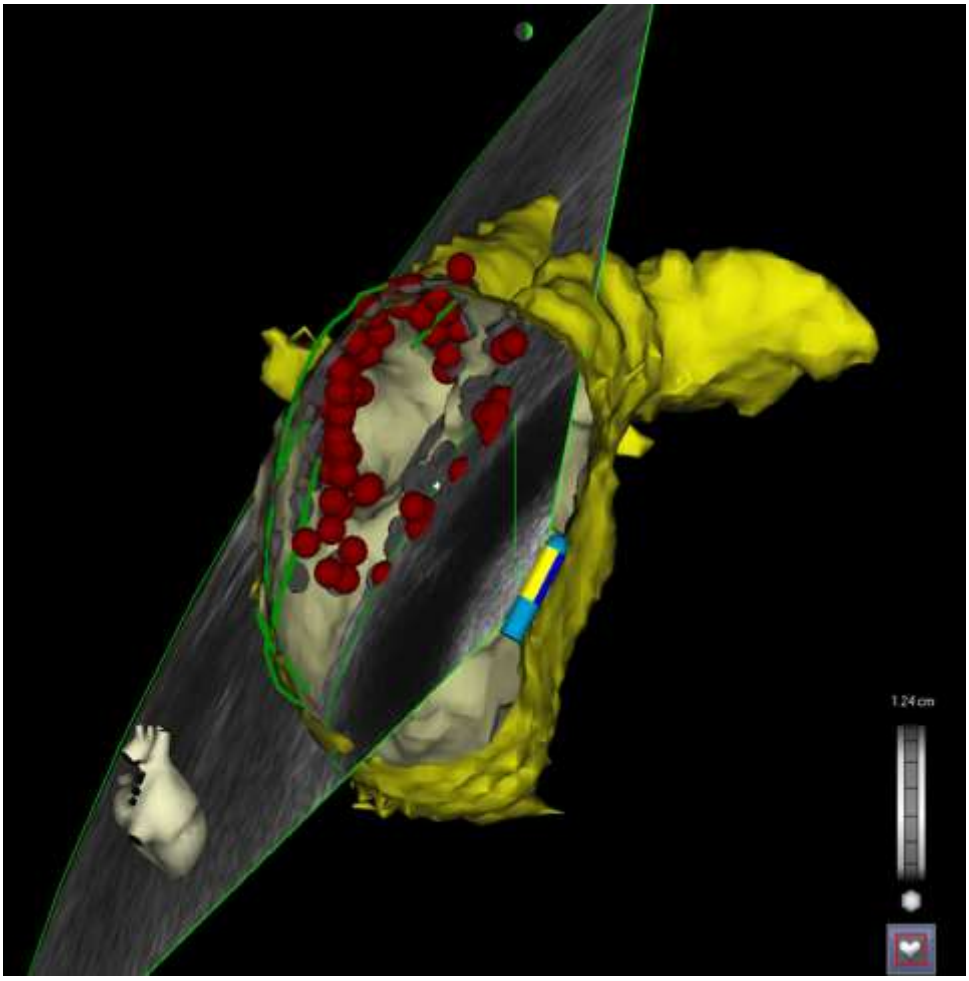

Figure 4. After registration the three-dimensional map created with intracardiac echocardiography and integrated multi-slice computed tomography image were used to facilitate the ablation procedure. Circumferential lesions were created outside the pulmonary vein ostia. Red tags represent the sites of radiofrequency current application.

Radiofrequency catheter ablation

Radiofrequency catheter ablation was performed by creating two circumferential lesions around the left and right PV antrum (Figure 4). Additional lesions consisting of a roofline, a mitral valve isthmus line or sites exhibiting fractionated activity were created if deemed necessary. After

excluding an intracardiac thrombus, and in the absence of a patent foramen ovale, a transseptal puncture was performed under ICE guidance. All patients received a bolus of intravenous heparin (5000 IU) with an additional bolus to maintain an activated clotting time between 300-400 s. The ablation procedure was guided by the 3D map created with ICE and integrated with the MSCT image. An open loop irrigated 4-mm tip quadripolar mapping/ablation catheter (7Fr Navistar™, Biosense Webster) was introduced in the LA and used to apply radiofrequency current outside the ostia of all PVs. At each point, radiofrequency current was applied at 30-35 W (maximum tip temperature 45 °C) until a voltage of <0.1 mV was achieved, with a maximum of 60 seconds per point.

Statistical analysis

Data are presented as mean ± SD or as number (percentage). Statistical analysis was performed using SPSS 14.0 software (SPSS Inc., Chicago, Illinois). Statistical comparisons were performed with two tailed Student's T-test, paired or unpaired as appropriate. Kappa analysis was used to quantify the level of agreement in PV anatomy classification with MSCT and ICE. Bland-Altman analysis was used to quantify the level of agreement between measurements of PV diameter with ICE and MSCT. A P value <0.05 was considered statistically significant.

Results

Study population

Seventeen patients were studied (13 men, mean age 56 ± 8 years). Atrial fibrillation was paroxysmal in 11 patients and persistent in 6 according to the ACC/AHA/ESC Guidelines definition [9]. Mean duration of AF was 72 ± 58 months

and the mean number of anti-arrhythmic drugs used was 3.7 ± 1.3 per patient. Mean LA size measured by transthoracic echocardiography was 41.8 ± 5.3 mm; mean left ventricular ejection fraction was 58 ± 7 %. Four patients had undergone another radiofrequency catheter ablation procedure for AF previously.

Table 1. Result of the registration process per patient

				Distance between contours and MSCT surface image (mm)		
Patient	Age (years)	Gender	No. of contours	Mean	SD	Range
1	46	F	20	2.1	1.6	0.00-8.45
2	55	M	19	1.9	1.4	0.00-8.91
3	61	M	27	2.3	1.6	0.00-8.82
4	72	M	23	2.5	1.9	0.01-10.27
5	57	M	18	2.1	1.7	0.01-10.17
6	40	F	36	1.8	1.4	0.01-7.19
7	58	M	39	2.6	1.9	0.00-9.99
8	48	M	38	2.0	1.5	0.00-7.68
9	61	F	29	1.9	1.4	0.15-6.45
10	47	M	42	1.7	1.4	0.00-7.44
11	68	M	22	2.3	1.5	0.01-7.03
12	50	M	40	2.1	1.6	0.01-9.15
13	53	F	38	1.9	1.7	0.00-12.50
14	58	M	31	2.8	1.9	0.02-11.56
15	60	M	43	2.5	1.8	0.00-8.57
16	54	M	30	2.5	1.7	0.01-8.36
17	58	M	34	2.3	1.6	0.01-8.38
Mean	55.6		31.1	2.2	1.7	
SD	8.0		8.5	0.3	0.2	

MSCT = multi-slice computed tomography, No. = number, SD = standard deviation.

Mapping and registration accuracy

In order to acquire a good geometry of LA and PVs a mean of 31.1 ± 8.5 ICE contours were drawn per patient (range 18-43 contours). The mean time needed to make a 3D map with ICE was 76 ± 27 minutes (range 25-126 minutes). It was noted that the time needed to make a map significantly decreased from 97 ± 20 minutes during the first 4 procedures to 39 ± 10

minutes during the last 13 procedures ($p<0.001$). After the registration process the mean distance between the drawn ICE contours and the MSCT surface image ranged from 1.7 to 2.8 mm (mean 2.2 ± 0.3 mm). The standard deviation of the ICE-MSCT difference ranged from 1.4 mm to 1.9 mm (mean 1.7 ± 0.2 mm). Individual results of the registration process are given in Table 1.

The accuracy of the registration process at the level of the PVs was evaluated by calculating the mean value of the distance between the contours and MSCT surface at 5 representative points around each PV ostium. The mean distance between the drawn contours and the MSCT surface image at the level of the PV ostia ranged from 0.7 to 4.4 mm (mean 1.7 ± 1.1 mm) and was smallest around the left inferior PV (mean 1.5 ± 1.1 mm) and largest around the left superior PV (mean 2.1 ± 1.3 mm) (Table 2).

Classification pulmonary vein anatomy

An equal number of 70 PVs were visualized with MSCT and ICE (4.12 ± 0.49 per patient). The most common PV variant consisted of 2 left sided PVs with separate ostia and 2 right sided PVs with separate ostia (7 patients, 41%). A common ostium of the left PVs was noted in 8 patients (47%) with MSCT and in 10 patients (59%) with ICE. A common trunk of the left superior and left inferior PV was recognized in 3 patients (18%) with both MSCT and ICE. An additional PV was identified in 5 patients (29%). All additional PVs were located at the right side of the LA. Using kappa analysis, an excellent agreement between MSCT and ICE for the classification of the left-sided PVs (kappa = 0.77) and the right-sided PVs (kappa = 1.00) was observed.

Table 2. Result of the registration process at pulmonary vein ostia

	Distance between contours and MSCT surface image (mm)		
Pulmonary vein	Mean	SD	Range
RSPV	1.7	1.0	0.8-3.2
RIPV	1.6	1.0	0.7-3.2
LSPV	2.1	1.3	0.8-4.4
LIPV	1.5	1.1	1.0-2.4
LCT	1.7	1.2	1.3-1.9
Both RPV	1.7	1.0	0.7-3.2
Both LPV	1.8	1.2	0.8-4.4
All PV	1.7	1.1	0.7-4.4

MSCT = multi-slice computed tomography, LCT = left common trunk, LIPV = left inferior pulmonary vein, LPV = left pulmonary veins, LSPV = left superior pulmonary vein, PV = pulmonary vein, RIPV = right pulmonary vein, RPV = right pulmonary veins, RSPV = right superior pulmonary vein, SD = standard deviation, SI = superior-inferior.

Quantitative measurements

Pulmonary vein diameters were measured in two directions on MSCT (AP and SI) and in the direction of the largest diameter possible on ICE, as previously described [4]. Superior-inferior diameters measured on MSCT were significantly larger for all PVs compared to the diameters measured on ICE (Table 3). The AP diameters of the right superior PV, left superior PV and additional veins measured on MSCT were not significantly different from the diameters measured on ICE. In contrast, the AP diameters of the right inferior PV on MSCT were significantly larger than the PV diameters on ICE (Table 3). Bland-Altman analysis demonstrated that there was a good overall agreement between ICE and MSCT for the assessment of the PV ostium diameter (Figure 5).

Left atrial diameter was measured in AP direction on both MSCT and ICE. Mean AP diameter of the LA on MSCT was 39.6 ± 7.2 mm compared to 35.9 ± 7.2 mm on ICE. The mean difference between AP diameter on MSCT and ICE was 3.7 ± 5.0 mm ($p<0.01$) and ranged from 0.3 to 15.6 mm.

Table 3. Measurements of pulmonary vein ostium diameter MSCT versus ICE

	MSCT SI (mm)	MSCT AP (mm)	ICE (mm)	SI diameter MSCT vs ICE (p-value)	AP diameter MSCT vs ICE (p-value)
RSPV	24.0 ± 3.5	19.2 ± 3.3	18.3 ± 3.3	<0.01	NS
RIPV	20.8 ± 3.0	17.9 ± 3.3	15.3 ± 2.4	<0.01	<0.05
LSPV	21.6 ± 3.9	15.4 ± 3.0	15.2 ± 2.2	<0.01	NS
LIPV	19.0 ± 2.1	11.9 ± 2.3	14.6 ± 2.4	<0.01	<0.05
LCT	38.2 ± 3.8	22.4 ± 1.0	28.2 ± 0.4	<0.05	<0.05
ADD	9.6 ± 1.9	8.5 ± 2.4	8.5 ± 0.9	<0.05	NS
All PV	21.5 ± 5.7	16.2 ± 4.5	16.0 ± 4.3	<0.01	NS

ADD = additional pulmonary vein, AP = anterior-posterior, ICE = intracardiac echocardiography, LCT = left common trunk, LIPV = left inferior pulmonary vein, LSPV = left superior pulmonary vein, MSCT = multi-slice computed tomography, PV = pulmonary vein, RIPV = right pulmonary vein, RSPV = right superior pulmonary vein, SI = superior-inferior

Radiofrequency catheter ablation

Transseptal puncture was performed under ICE guidance in 13 patients. A patent foramen ovale existed in 4 patients. The mean ablation time was 80 ± 34 minutes and mean fluoroscopy time was 35 ± 6 minutes. Radiofrequency catheter ablation was targeted at the PVs in all patients. No differences between heart rhythm during MSCT acquisition and ablation procedure were observed. No complications occurred during and after the ablation procedure.

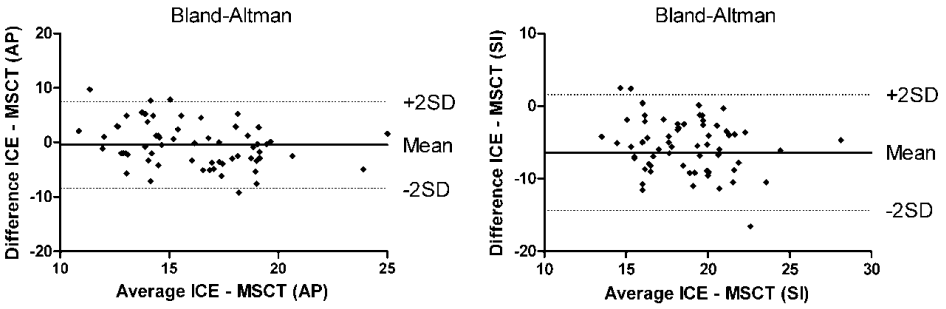

Figure 5. Bland-Altman analysis of measurements performed with multi-slice computed tomography and intracardiac echocardiography in anterior-posterior direction (left panel) and in superior-inferior (right panel) direction.

Discussion

The present study is the first to report on the feasibility of creating a 3D map of the LA and PVs with ICE and integrating this map with MSCT in order to facilitate RFCA for AF. This study has three main findings: 1) It is feasible to create an anatomical map of the LA and PVs using ICE contours; 2) The anatomical map created by ICE can accurately be merged with a MSCT surface image and 3) Anatomical ICE mapping is a sensitive imaging modality to visualize PVs and classify LA and PV anatomy.

3D mapping with ICE and MSCT integration

In the present study a novel mapping system was used that enables detection of a specifically designed ICE catheter with an imbedded CARTO navigation sensor. This mapping system allows acquisition of ECG gated ICE images and reconstructs them into a registered 3D shell. With this new technology, it has become possible to acquire accurate real-time anatomical information of the LA and PVs without entering the left side of the heart. Khaykin et al first reported on the use of 3D mapping with ICE during the ablation of a right free wall accessory pathway [10]. Okumura et al demonstrated the accuracy of navigation based on 3D mapping with ICE in animal experiments [11]. Both groups subsequently demonstrated the feasibility of creating a 3D map with ICE to guide RFCA for AF [11-13]. The present study supports these findings and additionally demonstrates the accuracy of creating a 3D map of the LA and PVs with ICE by comparing LA and PV geometry on the 3D ICE map with MSCT.

In addition, the current study is the first to demonstrate the feasibility of integrating a 3D map created with ICE and a MSCT image. Integration of MSCT images with conventional electroanatomical mapping is commonly used to guide RFCA for AF [14]. In an animal study, Dong et al [15] demonstrated that the integration of MSCT and electroanatomical mapping allows accurate

placement of anatomically guided ablation lesions in all cardiac chambers. Furthermore, several studies demonstrated the feasibility of the integration of MSCT and electroanatomical mapping to guide RFCA for AF [5,16-18]. Importantly, Kistler et al [6] showed that the integration of a MSCT image to guide RFCA for AF is associated with reduced fluoroscopy time and an improved outcome of the procedure.

However, the time interval between the MSCT data acquisition and the ablation procedure is a limitation of MSCT image integration. This delay may result in differences in heart rhythm, heart rate and fluid status which may cause errors in the image integration process, thereby compromising the accuracy of lesion placement. By integrating real-time ICE, MSCT and electroanatomical mapping, it has become possible to combine real-time anatomical and electrophysiological information with highly detailed anatomical information, thereby potentially increasing the accuracy of the placement of ablation lesions. The present study demonstrates the accuracy of integrating a MSCT image with a 3D map created with ICE. This was illustrated by a mean distance of only 2.2 mm between the MSCT image and the ICE contours, which is comparable with the integration results between an electroanatomical map and MSCT [5,16-18]. However, despite acquiring a good overall match between ICE and MSCT, the distance between the represented points along the ICE contours and MSCT ranged from 0.00 to 12.50 mm (Table 1). Similar ranges have been reported for the integration of electroanatomical maps and MSCT [5,16]. This wide range may be related to differences in reconstructed LA and PV anatomy between MSCT and ICE in areas that are strongly influenced by cardiac and respiratory movement.

Pulmonary vein visualization

Left atrial and PV anatomy are highly variable [3,4,19]. Importantly, accurate visualization of the PV ostia during RFCA for AF is required to avoid ablation within the PVs [2]. In the present study, the PV ostia were visualized with ICE and MSCT. Both imaging modalities recorded an equal number of PVs, which suggests that 3D mapping with ICE has a high sensitivity for detecting PVs. Furthermore, there was good agreement between ICE and MSCT for classification of the PV anatomy.

In the present study, ICE slightly underestimated PV diameter, as compared with MSCT. This observation is in agreement with a study by Jongbloed et al [4] who found that ICE underestimated PV diameter for all PVs by 3.5 mm in SI direction and 0.2 mm in AP direction. An explanation for the underestimation of left sided PV diameters on ICE may be the fact that these PVs are visualized in longitudinal cross-sections thereby potentially missing the middle and widest part of the PVs. In contrast, the underestimation of the right sided PV diameters may be due to the fact that the exact PV-LA junction can be challenging to visualize in transversal cross-sections. However, since radiofrequency current is typically applied outside the PVs, this should have little implications for the safety of the ablation procedure.

The present study shows that 3D mapping with ICE provides an accurate visualization of PV ostia and PV anatomy with a high sensitivity for detecting additional PVs and gives a good estimation of PV dimensions, as compared with MSCT.

Clinical implications

The integration of MSCT with electroanatomical mapping allows accurate placement of ablation lesions [15] and has improved the outcome of anatomically guided RFCA targeting the PVs [6]. However, it is reported that the accuracy of navigating with MSCT integration depends on the quality of the registration

process [7]. With the release of a new electroanatomical mapping system that allows integration of ICE it has become possible to acquire calibrated real-time 3D anatomical information without performing a manual registration process.

The ablation procedures in this study were guided by a 3D map made with ICE, integrated with a MSCT surface image. Importantly, this study demonstrates that 3D mapping with ICE alone provides accurate visualization of the LA geometry and PV ostia which is required to safely perform RFCA for AF targeting the PVs. Therefore it should be possible to perform an anatomically guided ablation procedure targeting the PVs on 3D mapping with ICE alone. This may result in a considerable reduction in radiation exposure for the patient. Further studies are therefore needed to fully explore the value of this promising new technique.

Limitations

This study represents an initial experience with 3D mapping using ICE to guide RFCA for AF. The time necessary to make a map with ICE was therefore relatively long. However, due to a clear learning curve, this time decreased in the later procedures. Therefore, it can be expected that the time needed to make a 3D ICE map can be shortened significantly.

In this study RFCA was guided by the 3D map made with ICE and integrated with the MSCT image. As a consequence no data has been acquired on guidance by 3D ICE mapping alone. Furthermore, at present no data is available on the outcome of the ablation procedures.

Intracardiac echocardiography allows real-time visualization of important cardiac structures. However, some areas of the LA may be challenging to visualize with ICE due to their parallel orientation to the ultrasound beam. Examples of these areas are the right sided PV-LA junction and the left side of the anterior wall. By positioning the ICE catheter inside the

right ventricle these structures can be visualized from another angle thereby providing more insight in LA and PV anatomy. Additionally, conventional electroanatomical mapping can also be used to acquire anatomical information in these and other areas.

Three-dimensional mapping with ICE is very sensitive to respiratory phase. Small differences in respiratory phase during image acquisition may result in contours situated outside the interpolated continuity of the other contours of the 3D map. However, by acquiring all ICE images during expiratory breath hold, consistent sets of contours could be acquired in all patients.

Three-dimensional mapping with ICE is a very promising but expensive technique. The ICE catheters used in this study are single-use only and a dedicated mapping system with image integration modules is needed to integrate ICE with the electroanatomical mapping and MSCT images. Furthermore this technology is only available on one electroanatomical mapping system (CARTO XP) and on limited echocardiographic machines (Sequoia ultrasound system and Cypress ultrasound system, Siemens Medical Solutions). Nonetheless, integration of ICE provides accurate anatomical information that could potentially replace MSCT integration in RFCA for AF. Replacing MSCT would render the use of ICE cost-efficient and would reduce radiation exposure to the patient. Furthermore, the ability to acquire registered real-time anatomical information of important structures with ICE has a significant additional value compared to MSCT integration.

Conclusions

Using a novel mapping system that allows integration of ICE and electroanatomical mapping it is feasible to create a real-time registered 3D

shell of LA and PV anatomy. Furthermore, the 3D map created with ICE can accurately be integrated with a MSCT surface image. This approach combines real-time anatomy with high detailed anatomy potentially providing highly accurate lesion placement during anatomical ablation procedures.

References

1. Haissaguerre M, Jais P, Shah DC, Takahashi A, Hocini M, Quiniou G, Garrigue S, Le MA, Le MP, Clementy J Spontaneous initiation of atrial fibrillation by ectopic beats originating in the pulmonary veins. N Engl J Med 1998;**339**:659-666.
2. Calkins H, Brugada J, Packer DL, Cappato R, Chen SA, Crijns HJ, Damiano RJ, Jr., Davies DW, Haines DE, Haissaguerre M, Iesaka Y, Jackman W, Jais P, Kottkamp H, Kuck KH, Lindsay BD, Marchlinski FE, McCarthy PM, Mont JL, Morady F, Nademanee K, Natale A, Pappone C, Prystowsky E, Raviele A, Ruskin JN, Shemin RJ HRS/EHRA/ECAS expert Consensus Statement on catheter and surgical ablation of atrial fibrillation: recommendations for personnel, policy, procedures and follow-up. A report of the Heart Rhythm Society (HRS) Task Force on catheter and surgical ablation of atrial fibrillation. Heart Rhythm 2007;**4**:816-861.
3. Mansour M, Holmvang G, Sosnovik D, Migrino R, Abbara S, Ruskin J, Keane D Assessment of pulmonary vein anatomic variability by magnetic resonance imaging: implications for catheter ablation techniques for atrial fibrillation. J Cardiovasc Electrophysiol 2004;**15**:387-393.
4. Jongbloed MR, Bax JJ, Lamb HJ, Dirksen MS, Zeppenfeld K, van der Wall EE, de RA, Schalij MJ Multislice computed tomography versus intracardiac echocardiography to evaluate the pulmonary veins before radiofrequency catheter ablation of atrial fibrillation: a head-to-head comparison. J Am Coll Cardiol 2005;**45**:343-350.
5. Tops LF, Bax JJ, Zeppenfeld K, Jongbloed MR, Lamb HJ, van der Wall EE, Schalij MJ Fusion of multislice computed tomography imaging with three-dimensional electroanatomic mapping to guide radiofrequency catheter ablation procedures. Heart Rhythm 2005;**2**:1076-1081.
6. Kistler PM, Rajappan K, Jahngir M, Earley MJ, Harris S, Abrams D, Gupta D, Liew R, Ellis S, Sporton SC, Schilling RJ The impact of CT image integration into an electroanatomic mapping system on clinical outcomes of catheter ablation of atrial fibrillation. J Cardiovasc Electrophysiol 2006;**17**:1093-1101.
7. Fahmy TS, Mlcochova H, Wazni OM, Patel D, Cihak R, Kanj M, Beheiry S, Burkhardt JD, Dresing T, Hao S, Tchou P, Kautzner J, Schweikert RA, Arruda M, Saliba W, Natale A Intracardiac echo-guided image integration: optimizing strategies for registration. J Cardiovasc Electrophysiol 2007;**18**:276-282.
8. Marom EM, Herndon JE, Kim YH, McAdams HP Variations in pulmonary venous drainage to the left atrium: implications for radiofrequency ablation. Radiology 2004;**230**:824-829.
9. Fuster V, Ryden LE, Cannom DS, Crijns HJ, Curtis AB, Ellenbogen KA, Halperin JL, Le Heuzey JY, Kay GN, Lowe JE, Olsson SB, Prystowsky EN, Tamargo JL, Wann S, Smith SC, Jr., Jacobs AK, Adams CD, Anderson JL, Antman EM, Hunt SA, Nishimura R, Ornato JP, Page RL, Riegel B, Priori SG, Blanc JJ, Budaj A, Camm AJ, Dean V, Deckers JW, Despres C, Dickstein K, Lekakis J, McGregor K, Metra M, Morais J, Osterspey A, Zamorano JL ACC/AHA/ESC 2006 guidelines for the management of patients with atrial fibrillation--executive summary: a report of the American College of Cardiology/American Heart Association Task Force on Practice Guidelines and the European Society of Cardiology Committee for Practice Guidelines (Writing Committee to Revise the 2001 Guidelines for the Management of Patients With Atrial Fibrillation). J Am Coll Cardiol 2006;**48**:854-906.
10. Khaykin Y, Klemm O, Verma A First human experience with real-time integration of intracardiac echocardiography and 3D electroanatomical imaging to guide right free wall accessory pathway ablation. Europace 2008;**10**:116-117.

11. Okumura Y, Henz BD, Johnson SB, Bunch TJ, O'Brien CJ, Hodge DO, Altman A, Govari A, Packer DL Three-Dimensional Ultrasound for Image-Guided Mapping and Intervention: Methods, Quantitative Validation, and Clinical Feasibility of a Novel Multimodality Image Mapping System. Circ Arrhythmia Electrophysiol 2008;**1**:110-119.
12. Khaykin, Y., Klemm, O., Whaley, B, Seabrook, C, Beardsall, M, Wulffhart, Z et al. First human experience with real time integration of intracardiac echocardiography and 3D electroanatomical imaging to guide pulmonary vein antrum isolation. J.Am.Coll.Cardiol. 51(10), A1-A34. 11-3-2008.
13. Khaykin, Y, Skanes, A, Wulffhart, Z, Gula, L, Whaley, B, Oosthuizen, R et al. Intracardiac ECHO Integration With Three Dimensional Mapping: Role in AF Ablation. JAFIB . 2008.
14. Tops LF, van der Wall EE, Schalij MJ, Bax JJ Multi-modality imaging to assess left atrial size, anatomy and function. Heart 2007;**93**:1461-1470.
15. Dong J, Calkins H, Solomon SB, Lai S, Dalal D, Lardo AC, Brem E, Preiss A, Berger RD, Halperin H, Dickfeld T Integrated electroanatomic mapping with three-dimensional computed tomographic images for real-time guided ablations. Circulation 2006;**113**:186-194.
16. Kistler PM, Earley MJ, Harris S, Abrams D, Ellis S, Sporton SC, Schilling RJ Validation of three-dimensional cardiac image integration: use of integrated CT image into electroanatomic mapping system to perform catheter ablation of atrial fibrillation. J Cardiovasc Electrophysiol 2006;**17**:341-348.
17. Martinek M, Nesser HJ, Aichinger J, Boehm G, Purerfellner H Accuracy of integration of multislice computed tomography imaging into three-dimensional electroanatomic mapping for real-time guided radiofrequency ablation of left atrial fibrillation-influence of heart rhythm and radiofrequency lesions. J Interv Card Electrophysiol 2006;**17**:85-92.
18. Dong J, Dalal D, Scherr D, Cheema A, Nazarian S, Bilchick K, Almasry I, Cheng A, Henrikson CA, Spragg D, Marine JE, Berger RD, Calkins H Impact of heart rhythm status on registration accuracy of the left atrium for catheter ablation of atrial fibrillation. J Cardiovasc Electrophysiol 2007;**18**:1269-1276.
19. Wood MA, Wittkamp M, Henry D, Martin R, Nixon JV, Shepard RK, Ellenbogen KA A comparison of pulmonary vein ostial anatomy by computerized tomography, echocardiography, and venography in patients with atrial fibrillation having radiofrequency catheter ablation. Am J Cardiol 2004;**93**:49-53.